SARS-CoV-2 Omicron spike mediated immune escape, infectivity and cell-cell fusion

Bo Meng[1,2], Isabella A.T.M Ferreira[1,2], Adam Abdullahi[1,2], Steven A. Kemp[1,2], Niluka Goonawardane [1,2], Guido Papa[3], Saman Fatihi[4], Oscar J. Charles[5], Dami Collier[1,2], CITIID-NIHR BioResource COVID-19 Collaboration, The Genotype to Phenotype Japan (G2P-Japan) Consortium, Jinwook Choi[6], Joo Hyeon Lee[6,7], Petra Mlcochova[1,2], Leo James[3], Rainer Doffinger[2], Lipika Thukral[4], Kei Sato[8,9*], Ravindra K Gupta[1,2,10]*

[1] Cambridge Institute of Therapeutic Immunology & Infectious Disease (CITIID), Cambridge, UK.
[2] Department of Medicine, University of Cambridge, Cambridge, UK.
[3] MRC – Laboratory of Molecular Biology, Cambridge, UK.
[4] CSIR Institute of Genomics and Integrative Biology, Delhi, India
[5] Division of Infection and Immunity, UCL, London
[6] Wellcome-MRC Cambridge Stem Cell Institute, Cambridge, UK.
[7]Department of Physiology, Development and Neuroscience, University of Cambridge, Cambridge, UK.
[8] Division of Systems Virology, The Institute of Medical Science, The University of Tokyo, Tokyo 1088639, Japan
[9] CREST, Japan Science and Technology Agency, Saitama 3220012, Japan
[10]Africa Health Research Institute, Durban, South Africa.

*Address for correspondence:
rkg20@cam.ac.uk; keisato@g.ecc.u-tokyo.ac.jp

Key words: SARS-CoV-2; COVID-19; Omicron variant; B.1.1.529; antibody escape; neutralising antibodies; infectivity; spike mutation; evasion; resistance; fitness; fusion; syncytia, ChAdOx-1, BNT162b.

Abstract

The Omicron variant emerged in southern Africa in late 2021 and is characterised by multiple spike mutations across all spike domains. Here we show that the Omicron spike confers very significant evasion of vaccine elicited neutralising antibodies that is more pronounced for ChAdOx-1 adenovirus vectored vaccine versus BNT162b2 mRNA vaccine. Indeed neutralisation of Omicron was not detectable for the majority of individuals who had received two doses of ChAdOx-1. Third dose mRNA vaccination rescues neutralisation in the short term. Despite three mutations predicted to favour spike S1/S2 cleavage, observed cleavage efficiency is lower than for wild type Wuhan-1 D614G and Delta. We demonstrate significantly lower infectivity of lung organoids and Calu-3 lung cells expressing endogenous levels of ACE2 and TMPRSS2 but similar infection as compared to Delta when using H1299 lung epithelial cells. Importantly, fusogenicity of the Omicron spike is significantly impaired, leading to marked reduction in syncitia formation. These observations highlight that Omicron has gained immune evasion properties whilst compromising on properties associated with replication and pathogenicity.

Introduction

The Omicron variant was first detected in South Africa and has now spread internationally[1]. It has been associated with very rapid increases in case numbers and recent data demonstrate significant evasion of neutralising antibody responses[1]. Omicron appears to be competing with the Delta variant in the UK and this may be due to an advantage in vaccinated / previously exposed populations and/or increased replication. Data on replication are limited however. Delta spike was previously shown to confer more efficient cell-cell fusion kinetics compared to Wuhan-1[2], and syncytia formation has previously been associated with pathogenesis[3]. Moreover, changes in the PBCS have been associated with pathogenicity. Omicron has three mutations in the furin cleavage site region (P681H, H655Y and N679K) and has therefore been predicted to be highly infectious and fit.

Here we show that contrary to predictions based on mutational profiling of the PBCS region, Omicron spike is relatively poorly cleaved, and impaired in mediating cell-cell fusion and syncytia formation. This reduced cleavage is also associated with poorer entry into target lung organoids or cell lines expressing endogenous levels of receptors. We also show that as expected from mutational profiling, omicron has significantly reduced sensitivity to

neutralising antibodies and that AZ vaccine sera display lower titres as compared to mRNA vaccine sera. Soon after a third dose with mRNA however, robust titres against Omicron can be achieved, thus supporting third dose 'boosting' strategies.

Results

The Omicron spike protein shows increased intramolecular bonding, changes in charged residues and multiple mutations across domains.

We first sought to investigate the distribution of mutations and their impacts. We observed increased intramolecular hydrogen bonds in Delta and Omicron compared with Wu-1 (Figure 1a). In addition when we simulated interactions with ACE2 Omicron displayed multiple contacts with ACE2 in contrast to Delta and Wu-1 (Figure 1b). When charge at the protein surface was modelled there was again a striking difference between Omicron and earlier variants, in particular with positive charge accumulating in the RBD (Figure 1c).

Omicron spike protein confers broad escape from two dose vaccination with adenovirus vectored and mRNA vaccines

We next synthesised codon optimised spike expression plasmids for Omicron and Delta spike proteins and generated PV particles. We obtained longitudinal serum samples from individuals vaccinated with either BNT162b2 or ChAdOx-1 vaccines. We observed more than ten-fold loss of neutralisation against Omicron after the second dose compared to Delta. Indeed neutralisation of Omicron was not detectable for the majority of individuals who had received two doses of ChAdOx-1. We additionally also observed waning over time since second dose (Figure 3). Both groups were boosted with BNT162b2 as a third dose, allowing us to compare the response to this boosting dose. Significant increases in neutralisation were observed for all variants tested, suggesting increased breadth of responses as well as titre.

Omicron Spike protein induces relatively poor cell-cell fusion compared to Delta

Mutations at P681 in the PBCS have been observed in multiple SARS-CoV-2 lineages, most notably in the B.1.1.7 Alpha variant[4] and the Delta variant. We previously showed that these

spikes, bearing P681 mutations, had significantly higher fusogenic potential than a D614G Wuhan-1 spike [5]. Omicron bears P681H, in addition to 679 and 655 mutations (**Figure 4a**). We tested Omicron spike using a split GFP system to monitor cell-cell fusion (**Figure 4b**). We transfected spike bearing plasmids into Vero cells stably expressing the two different part of Split-GFP, so that GFP signal could be measured over time upon cell-cell fusion (**Figure 4b,c**). We observed increased fusion for Delta as compared to D614G Wuhan-1 spike as shown previously. The Omicron spike however resulted in very poor fusion (**Figure 4d)**, despite being expressed (**Figure 4e**).

Omicron Spike protein mediates deficient cell entry in lung alveolar organoids

Spike mediates cell entry via interaction with ACE2 and TMPRSS2[6] and is a major determinant of viral infectivity. The plasma membrane route of entry, and indeed transmissibility in animal models, is critically dependent on the polybasic cleavage site (PBCS) between S1 and S2[7-9]and cleavage of spike prior to virion release from producer cells; this contrasts with the endosomal entry route, which does not require spike cleavage in producer cells. [5,8,10]. Plasma membrane fusion allows the virus to avoid restriction factors in endosomes[8].

We tested single round viral entry of Wuhan-1 D614G, Delta and Omicron spikes (Figure 5) using the PV system, infecting primary 3D lung alveolar organoids (Figure 5a,b) and Calu-3 lung cells (Figure 5c) expressing endogenous levels of ACE2 and TMPRSS2, as well as the A549 lung cell line transduced with ACE2 and TMPRSS2 (Figure 5d). We first probed PV virions for spike protein and noted that the Omicron spike was predominantly in the uncleaved form, in contrast to Delta and WT (Figure 5a). We observed variable entry efficiency for Omicron in comparison to Delta and Wuhan-1 D614G wild type. SARS-CoV-2 infection in organoids and Calu-3 lung cells (that do not overexpress receptors ACE2 and TMPRSS2) was impaired for Omicron relative to Delta and Wuhan D614G. Interestingly Calu-3 do not express Cathepsin and therefore entry is entirely plasma membrane dependent. We speculate that the impaired infection in cathepsin deficient Calu-3 cells relative to Delta may relate to relatively lower spike cleavage as compared to Delta. By contrast, in H1299 lung epithelial cells we observed similar entry efficiency for Delta and Omicron (Figure 5e).

Discussion

Here we have shown that the Omicron spike confers very significant evasion of vaccine elicited neutralising antibodies that is more dramatic for ChAdOx-1 versus BNT162b2 vaccine sera. These data are supported by vaccine effectiveness measurements in the UK (UKHSA report Dec 2021). Third dose mRNA vaccination rescued neutralisation in the short term, though waning is expected to occur over time.

Importantly, we show that despite three mutations predicted to favour spike S1/S2 cleavage, observed cleavage efficiency is similar to wild type Wuhan-1 D614G and lower than Delta. As expected from suboptimal cleavage, we show poor fusogenic potential of the Omicron spike when expressed in cells. This phenomenon could translate to impaired cell-cell spread, and indeed investigators have observed smaller plaque sizes (personal communication). Omicron spike was also associated with poorer entry into target lung organoids or Calu-3 lung cell lines expressing endogenous levels of receptors.

These observations highlight that Omicron has gained immune evasion properties whilst compromising syncitia formation and cell entry in lung cells, with possible implications for pathogenicity. Critically, ChAdOx-1 is widely used in low income settings where third doses with mRNA not widely available, and Omicron may contribute to severe disease in such settings.

Methods

Serum samples and ethical approval

Ethical approval for study of vaccine elicited antibodies in sera from vaccinees was obtained from the East of England – Cambridge Central Research Ethics Committee Cambridge (REC ref: 17/EE/0025). Use of convalescent sera had ethical approval from South Central Berkshire B Research Ethics Committee (REC ref: 20/SC/0206; IRAS 283805). Studies involving health care workers (including testing and sequencing of respiratory samples) were reviewed and approved by The Institutional Human Ethics Committees of NCDC and CSIR-IGIB(NCDC/2020/NERC/14 and CSIR-IGIB/IHEC/2020-21/01). Participants provided informed consent.

Sequencing

Spike genomes for the original Wuhan strain, and Omicron VOC were obtained from GISAID EpiCoV database accessed on 30th November 2021. A consensus Spike genome was created from all complete and high coverage genomes, excluding all sequences with >5% Ns using Geneious Prime v2022. The consensus genome was translated to poly-proteins and the Spike gene was aligned to the original Wuhan strain using mafft v7.490[11] with the --globalpair --maxiterate 1000 flags.

Structural analysis

3D structural models of the spike homotrimer protein complex were generated using Alphafold v2.1.1[12]. In its validation at the 14th edition of the Critical Assessment of protein Structure Prediction (CASP14) the predictions generated were demonstrated to be comparative to experimental structures. When a close homolog structure is available to Alphafold the predictions it generates for those positions are within typical experimental error. Required databases were downloaded on 02/12/2021. The program was run with the parameters --max_template_date=2021-12-01 --model_preset=monomer --db_preset=full_dbs --is_prokaryote_list=false. Protein structures were visualised in ChimeraX v1.3[13]. As predicted structures for the whole spike protein include poorly resolved chains at the terminal ends, these residues were identified by overlaying structures on PDB entry 6ZP2, then selected and removed from PDB files using the delete atoms/bonds action. Two further monomers were overlayed on 6zp2 to generate a homotrimer structure. Mutated residues were then coloured in red and labelled manually with respect to the Wuhan strain.

Data availability:

All protein structures shown are freely available at github.com/ojcharles/viral_alphafold

Pseudotype virus experiments

Cells

HEK 293T CRL-3216, Hela-ACE-2 (Gift from James Voss), Vero CCL-81 were maintained in Dulbecco's Modified Eagle Medium (DMEM) supplemented with 10% fetal calf serum (FCS), 100 U/ml penicillin, and 100mg/ml streptomycin. All cells were regularly tested and are mycoplasma free. H1299 cells were a kind gift from Sam Cook. Calu-3 cells were a kind gift from Paul Lehner, A549 A2T2[14] cells were a kind gift from Massimo Palmerini. Vero E6 Ace2/TMPRSS2 cells were a kind gift from Emma Thomson.

Pseudotype virus preparation for testing against vaccine elicited antibodies and cell entry

Plasmids encoding the spike protein of SARS-CoV-2 D614 with a C terminal 19 amino acid deletion with D614G were used. Omicron and Delta spikes were generated by gene synthesis. Viral vectors were prepared by transfection of 293T cells by using Fugene HD transfection reagent (Promega). 293T cells were transfected with a mixture of 11ul of Fugene HD, 1µg of pCDNAΔ19 spike-HA, 1ug of p8.91 HIV-1 gag-pol expression vector and 1.5µg of pCSFLW (expressing the firefly luciferase reporter gene with the HIV-1 packaging signal). Viral supernatant was collected at 48 and 72h after transfection, filtered through 0.45um filter and stored at -80˚C as previously described. Infectivity was measured by luciferase detection in target 293T cells transfected with TMPRSS2 and ACE2.

Standardisation of virus input by SYBR Green-based product-enhanced PCR assay (SG-PERT)

The reverse transcriptase activity of virus preparations was determined by qPCR using a SYBR Green-based product-enhanced PCR assay (SG-PERT) as previously described[15]. Briefly, 10-fold dilutions of virus supernatant were lysed in a 1:1 ratio in a 2x lysis solution (made up of 40% glycerol v/v 0.25% Triton X-100 v/v 100mM KCl, RNase inhibitor 0.8 U/ml, TrisHCL 100mM, buffered to pH7.4) for 10 minutes at room temperature.

12µl of each sample lysate was added to thirteen 13µl of a SYBR Green master mix (containing 0.5µM of MS2-RNA Fwd and Rev primers, 3.5pmol/ml of MS2-RNA, and 0.125U/µl of Ribolock RNAse inhibitor and cycled in a QuantStudio. Relative amounts of reverse transcriptase activity were determined as the rate of transcription of bacteriophage MS2 RNA, with absolute RT activity calculated by comparing the relative amounts of RT to an RT standard of known activity.

Neutralisation titre analyses

The neutralisation by vaccine-elicited antibodies after two doses of the BNT162b2 and Chad-Ox-1 vaccine, as well as after a third dose with BNT162b2 was determined by infections in the presence of serial dilutions of sera as described below. The ID50 within groups were summarised as a geometric mean titre (GMT) and statistical comparison between groups were made with Mann-Whitney or Wilcoxon ranked sign test. Statistical analyses were done using Stata v13 and Prism v9.

Western blotting

Cells were lysed and supernatants collected 18 hours post transfection. Purified virions were prepared by harvesting supernatants and passing through a 0.45 μm filter. Clarified supernatants were then loaded onto a thin layer of 8.4% optiprep density gradient medium (Sigma-Aldrich) and placed in a TLA55 rotor (Beckman Coulter) for ultracentrifugation for 2 hours at 20,000 rpm. The pellet was then resuspended for western blotting. Cells were lysed with cell lysis buffer (Cell signalling), treated with Benzonase Nuclease (70664 Millipore) and boiled for 5 min. Samples were then run on 4%–12% Bis Tris gels and transferred onto nitrocellulose or PVDF membranes using an iBlot or semidry (Life Technologies and Biorad, respectively).

Membranes were blocked for 1 hour in 5% non-fat milk in PBS + 0.1% Tween-20 (PBST) at room temperature with agitation, incubated in primary antibody (anti-SARS-CoV-2 Spike, which detects the S2 subunit of SARS-CoV-2 S (Invitrogen, PA1-41165), anti-GAPDH (proteintech) or anti-p24 (NIBSC)) diluted in 5% non-fat milk in PBST for 2 hours at 4°C with agitation, washed four times in PBST for 5 minutes at room temperature with agitation and incubated in secondary antibodies anti-rabbit HRP (1:10000, Invitrogen 31462), anti-bactin HRP (1:5000; sc-47778) diluted in 5% non-fat milk in PBST for 1 hour with agitation at room temperature. Membranes were washed four times in PBST for 5 minutes at room temperature and imaged directly using a ChemiDoc MP imaging system (Bio-Rad).

Plasmids for split GFP system to measure cell-cell fusion

pQCXIP-BSR-GFP11 and pQCXIP-GFP1-10 were from Yutaka Hata [16] Addgene plasmid #68716; http://n2t.net/addgene:68716; RRID:Addgene_68716 and Addgene plasmid #68715; http://n2t.net/addgene:68715; RRID:Addgene_68715)

Generation of GFP1-10 or GFP11 lentiviral particles

Lentiviral particles were generated by co-transfection of Vero cells with pQCXIP-BSR-GFP11 or pQCXIP-GFP1-10 as previously described [17]. Supernatant containing virus particles was harvested after 48 and 72 hours, 0.45 μm filtered, and used to infect 293T or Vero cells to generate stable cell lines. 293T and Vero cells were transduced to stably express GFP1-10 or GFP11 respectively and were selected with 2 μg/ml puromycin.

Cell-cell fusion assay

Cell-cell fusion assay was carried out as previously described [17,18] but using a Split-GFP system. Briefly, Vero GFP1-10 and Vero-GFP11 cells were seeded at 80% confluence in a 1:1 ration in 24 multiwell plate the day before. Cells. were co-transfected with 0.5 µg of spike expression plasmids in pCDNA3 using Fugene 6 and following the manufacturer's instructions (Promega). Cell-cell fusion was measured using an Incucyte and determined as the proportion of green area to total phase area. Data were then analysed using Incucyte software analysis. Graphs were generated using Prism 8 software.

Acknowledgments

RKG is supported by a Wellcome Trust Senior Fellowship in Clinical Science (WT108082AIA). This study was supported by the Cambridge NIHRB Biomedical Research Centre. I.A.T.M.F. is funded by a SANTHE award (DEL-15-006). We would like to thank Paul Lehner for Calu-3 cells. We would like to thank James Voss for HeLa ACE2 and Suzanne Rihn for the A549 cells. Davide Corti for the Omicron spike plasmid. We thank the Geno2pheno UK consortium. The authors acknowledge support from the G2P-UK National Virology consortium funded by MRC/UKRI (grant ref: MR/W005611/1).This study was also supported by The Rosetrees Trust and the Geno2pheno UK consortium. SF acknowledges the EPSRC (EP/V002910/1). KS is supported by AMED Research Program on Emerging and Re-emerging Infectious Diseases (20fk0108270 and 20fk0108413), JST SICORP (JPMJSC20U1 and JPMJSC21U5) and JST CREST (JPMJCR20H4).

References

1 Cele, S. *et al.* SARS-CoV-2 Omicron has extensive but incomplete escape of Pfizer BNT162b2 elicited neutralization and requires ACE2 for infection. *medRxiv*, 2021.2012.2008.21267417, doi:10.1101/2021.12.08.21267417 (2021).

2 Mlcochova, P. *et al.* SARS-CoV-2 B.1.617.2 Delta variant replication and immune evasion. *Nature* **599**, 114-119, doi:10.1038/s41586-021-03944-y (2021).

3 Saito, A. *et al.* Enhanced fusogenicity and pathogenicity of SARS-CoV-2 Delta P681R mutation. *Nature*, doi:10.1038/s41586-021-04266-9 (2021).

4 Kemp, S. *et al.* Recurrent emergence and transmission of a SARS-CoV-2 Spike deletion H69/V70. *bioRxiv*, 2020.2012.2014.422555, doi:10.1101/2020.12.14.422555 (2021).

5 Meng, B. *et al.* Recurrent emergence and transmission of a SARS-CoV-2 spike deletion H69/V70 and role in Alpha Variant B.1.1.7. *Cell reports*, doi:https://doi.org/10.1016/j.celrep.2021.109292 (2021).

6 Hoffmann, M. *et al.* SARS-CoV-2 Cell Entry Depends on ACE2 and TMPRSS2 and Is Blocked by a Clinically Proven Protease Inhibitor. *Cell* **181**, 271-280 e278, doi:10.1016/j.cell.2020.02.052 (2020).
7 Papa, G. *et al.* Furin cleavage of SARS-CoV-2 Spike promotes but is not essential for infection and cell-cell fusion. *PLoS pathogens* **17**, e1009246, doi:10.1371/journal.ppat.1009246 (2021).
8 Peacock, T. P. *et al.* The furin cleavage site in the SARS-CoV-2 spike protein is required for transmission in ferrets. *Nat Microbiol*, doi:10.1038/s41564-021-00908-w (2021).
9 Cattin-Ortolá, J. *et al.* Sequences in the cytoplasmic tail of SARS-CoV-2 Spike facilitate expression at the cell surface and syncytia formation. *bioRxiv*, 2020.2010.2012.335562, doi:10.1101/2020.10.12.335562 (2021).
10 Winstone, H. *et al.* The Polybasic Cleavage Site in SARS-CoV-2 Spike Modulates Viral Sensitivity to Type I Interferon and IFITM2. *Journal of virology* **95**, e02422-02420, doi:10.1128/jvi.02422-20 (2021).
11 Katoh, K. & Standley, D. M. MAFFT multiple sequence alignment software version 7: improvements in performance and usability. *Mol Biol Evol* **30**, 772-780, doi:10.1093/molbev/mst010 (2013).
12 Jumper, J. *et al.* Highly accurate protein structure prediction with AlphaFold. *Nature* **596**, 583-589, doi:10.1038/s41586-021-03819-2 (2021).
13 Goddard, T. D. *et al.* UCSF ChimeraX: Meeting modern challenges in visualization and analysis. *Protein Science* **27**, 14-25 (2018).
14 Rihn, S. J. *et al.* A plasmid DNA-launched SARS-CoV-2 reverse genetics system and coronavirus toolkit for COVID-19 research. *PLoS Biol* **19**, e3001091, doi:10.1371/journal.pbio.3001091 (2021).
15 Vermeire, J. *et al.* Quantification of reverse transcriptase activity by real-time PCR as a fast and accurate method for titration of HIV, lenti- and retroviral vectors. *PloS one* **7**, e50859-e50859, doi:10.1371/journal.pone.0050859 (2012).
16 Kodaka, M. *et al.* A new cell-based assay to evaluate myogenesis in mouse myoblast C2C12 cells. *Experimental cell research* **336**, 171-181 (2015).
17 Papa, G. *et al.* Furin cleavage of SARS-CoV-2 Spike promotes but is not essential for infection and cell-cell fusion. *PLoS Pathogens* **17**, e1009246 (2021).
18 Buchrieser, J. *et al.* Syncytia formation by SARS-CoV-2-infected cells. *The EMBO journal* **39**, e106267 (2020).

The Genotype to Phenotype Japan (G2P-Japan) Consortium members

Ryoko Kawabata[16], Nanami Morizako[16] , Kenji Sadamasu[17], Hiroyuki Asakura[17], Mami Nagashima[17], Kazuhisa Yoshimura[17], Jumpei Ito[18], Izumi Kimura[18], Keiya Uriu[18], Yusuke Kosugi[18], Mai Suganami[18], Akiko Oide[18], Miyabishara Yokoyama[18], Mika Chiba[18] , Akatsuki Saito[31], Erika P Butlertanaka[31], Yuri L Tanaka[31], Terumasa Ikeda[32], Chihiro Motozono[32],

Hesham Nasser[32], Ryo Shimizu[32], Yue Yuan[32], Kazuko Kitazato[32], Haruyo Hasebe[32] , So Nakagawa[33], Jiaqi Wu[33], Miyoko Takahashi[33], Takasuke Fukuhara[34], Kenta Shimizu[34], Kana Tsushima[34], Haruko Kubo[34], Kotaro Shirakawa[35], Yasuhiro Kazuma[35], Ryosuke Nomura[35], Yoshihito Horisawa[35], Akifumi Takaori-Kondo[35], Kenzo Tokunaga[36], Seiya Ozono[36]

[31]University of Miyazaki, Miyazaki, Japan
[32]Kumamoto University, Kumamoto, Japan
[33]Tokai University, Tokyo, Japan
[34]Hokkaido University, Sapporo, Japan
[35]Kyoto University, Kyoto, Japan
[36]National Institute of Infectious Diseases, Tokyo, Japan

The CITIID-NIHR BioResource COVID-19 Collaboration

Stephen Baker[1,2], Gordon Dougan[1,2] , Christoph Hess[2], Nathalie Kingston[9], Paul J. Lehner[1,2], Paul A. Lyons[1,2], Nicholas J. Matheson[1,2], Willem H. Owehand[22], Caroline Saunders[21], Charlotte Summers[2] , James E.D. Thaventhiran[2], Mark Toshner[2], Michael P. Weekes[2], Patrick Maxwell[37], Ashley Shaw[37]

Ashlea Bucke[38], Jo Calder[38], Laura Canna[38], Jason Domingo[38], Anne Elmer[38], Stewart Fuller[38], Julie Harris[38], Sarah Hewitt[38], Jane Kennet[38], Sherly Jose[38], Jenny Kourampa[38], Anne Meadows[38], Criona O'Brien[38], Jane Price[38], Cherry Publico[38], Rebecca Rastall[38], Carla Ribeiro[38], Jane Rowlands[38], Valentina Ruffolo[38], Hugo Tordesillas[38], Ben Bullman[1], Benjamin J. Dunmore[2], Stuart Fawke[39], Stefan Gräf [2], Josh Hodgson[3], Christopher Huang[3], Kelvin Hunter[2,], Emma Jones[31], Ekaterina Legchenko[2], Cecilia Matara[2], Jennifer Martin[2], Federica Mescia[2], Ciara O'Donnell[2], Linda Pointon[2], Nicole Pond[2], Joy Shih[2], Rachel Sutcliffe[2], Tobias Tilly[2], Carmen Treacy[2], Zhen Tong[2], Jennifer Wood[2], Marta Wylot[2], Laura Bergamaschi[2], Ariana Betancourt[2], Georgie Bower[2], Chiara Cossetti[2,], Aloka De Sa[2], Madeline Epping[2], Stuart Fawke[2]**,** Nick Gleadall[2], Richard Grenfell[2], Andrew Hinch[2], Oisin Huhn[39], Sarah Jackson[2], Isobel Jarvis[2], Ben Krishna[2], Daniel Lewis[3], Joe Marsden[3], Francesca Nice[41], Georgina Okecha[3], Ommar Omarjee[2], Marianne Perera[2], Martin Potts[2], Nathan Richoz[2], Veronika Romashova[2], Natalia Savinykh Yarkoni[3], Rahul Sharma[3], Luca Stefanucci[2], Jonathan Stephens[22], Mateusz Strezlecki[2], Lori Turner[2], Eckart M.D.D. De Bie[2], Katherine Bunclark[2], Masa Josipovic[2], Michael Mackay[2], Federica Mescia[2], Alice Michael[27], Sabrina Rossi[37], Mayurun Selvan[3], Sarah Spencer[15], Cissy Yong[37], John Allison[9], Helen

Butcher[9,40], Daniela Caputo[9,40], Debbie Clapham-Riley[9,40], Eleanor Dewhurst[9,40], Anita Furlong[9,40], Barbara Graves[9,40], Jennifer Gray[9,40], Tasmin Ivers[9,40], Mary Kasanicki[9,30], Emma Le Gresley[9,40], Rachel Linger[9,40], Sarah Meloy[9,40], Francesca Muldoon[9,40], Nigel Ovington[9], Sofia Papadia[9,40], Isabel Phelan[9,40], Hannah Stark[9,40], Kathleen E Stirrups[22,12], Paul Townsend[40], Neil Walker[40], Jennifer Webster[9,40], Ingrid Scholtes[40], Sabine Hein[40], Rebecca King[40]

[37] Cambridge University Hospitals NHS Trust, Cambridge UK.
[38]Cambridge Clinical Research Centre, NIHR Clinical Research Facility, Cambridge University Hospitals NHS Foundation Trust, Addenbrooke's Hospital, Cambridge CB2 0QQ, UK
[39]Department of Biochemistry, University of Cambridge, Cambridge, CB2 1QW, UK
[40]University of Cambridge, Cambridge Biomedical Campus, Cambridge CB2 0QQ, UK

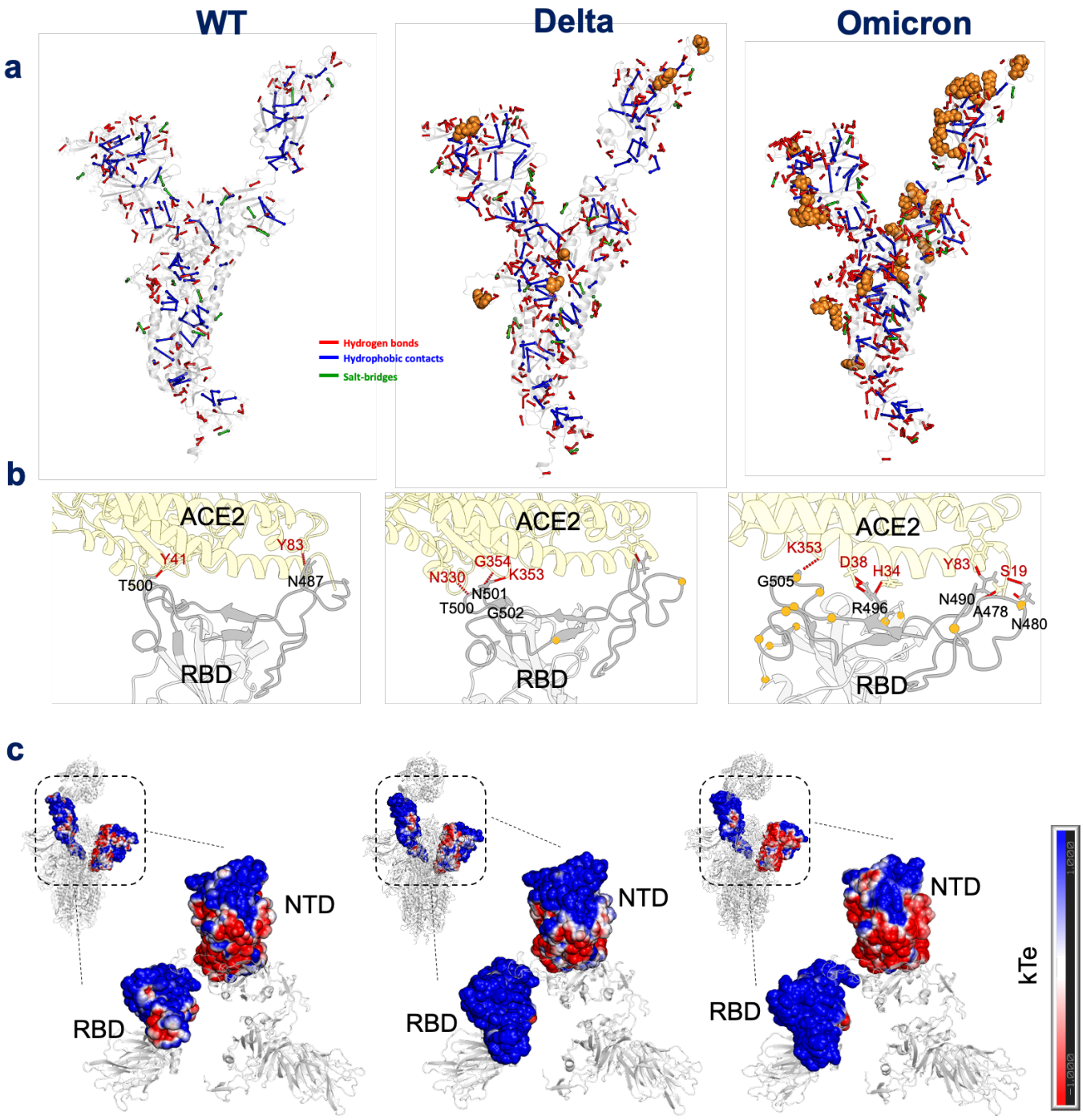

Figure 1: Intra-protein interaction network of WT, DELTA and OMICRON spike. a. Comparative global intra-molecular network for WT ,Delta and omicron spike **structural model** protein calculated throughout 100ns simulation length and interactions with >50% persistence are shown. For clarity only unique hydrogen bonds specific to each variant spike protein are marked in red on one of the chains of spike trimer. The total number of salt bridges and hydrophobic contacts are highlighted in green and blue, respectively and the mutations present in Delta and Omicron are marked in yellow spheres. **b**. The zoomed-in structural map shows a hydrogen bonding pattern at a static structure (50ns) around the mutation sites in the RBD **c** Electrostatic surface of the spike NTD and RBD regions. Blue denotes positive charge potential, while red indicates negative charge potential. The potential distribution was calculated by APBS. The values range from –1k*T*(red) to 0 (white) and to +1k*T* (blue), where *T* is the temperature, and k is the Boltzmann constant.

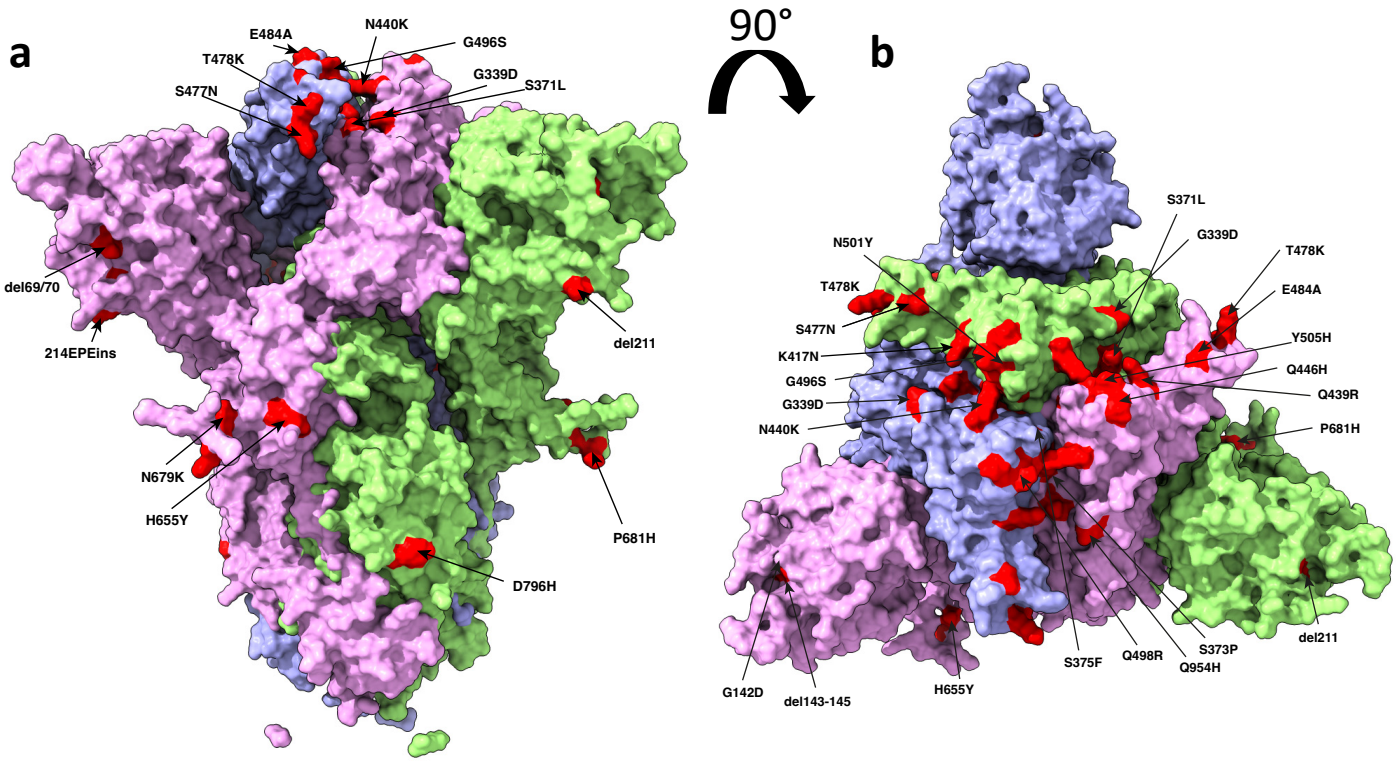

Figure 2. a. Side Surface representation of the Omicron B.A1 spike protein. b. Top down view surface representation of the Omicron BA.1 spike protein. Spike homotrimer structures were created predicted *in silico* by the Alphafold2 software package. Individual mutations making up the Omicron spike are highlighted in red on each of the three homotrimers.

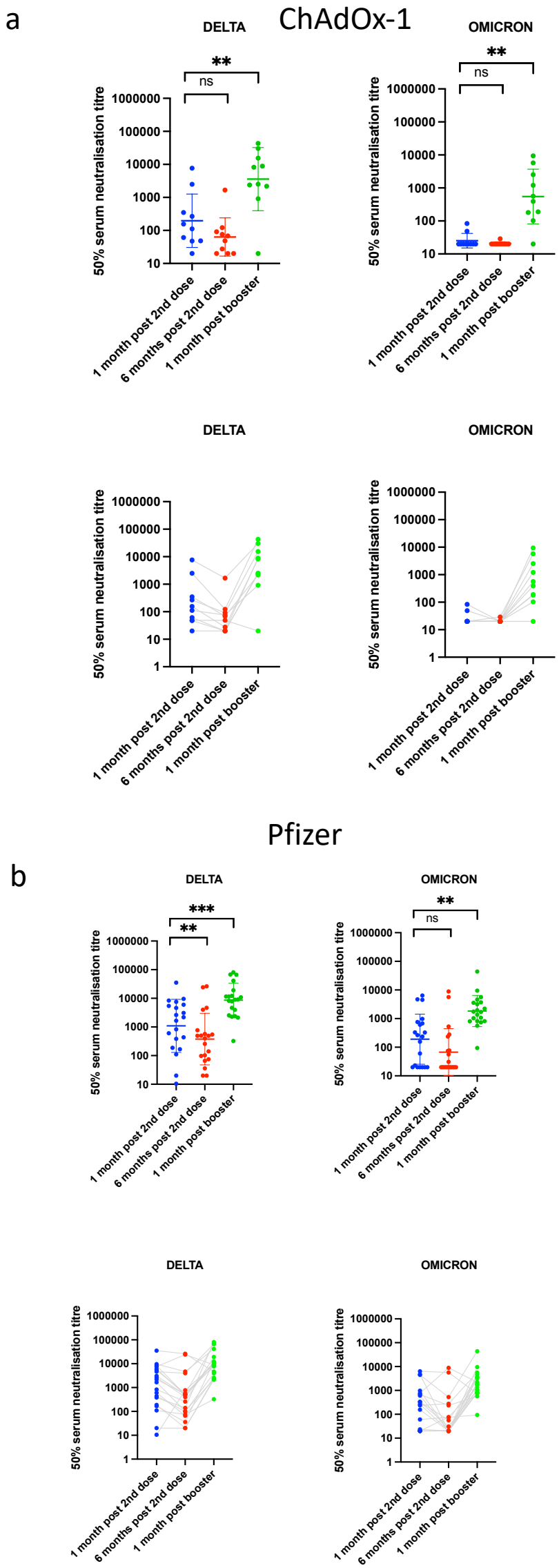

Figure 3: Neutralisation of spike pseudotyped virus by sera from vaccinated individuals over three longitudinal time points following doses two (AZ or Pfizer) and three (Pfizer only) a,b n=20 ChAdOx-1 or c,d n=20 BNT12b2. GMT (geometric mean titre) with s.d are presented. Data representative of two independent experiments each with two technical replicates. N antibody positive individuals were excluded from this analysis. **p<0.01, *** p<0.001, ****p<0.0001 Wilcoxon matched-pairs signed rank test, ns not significant.

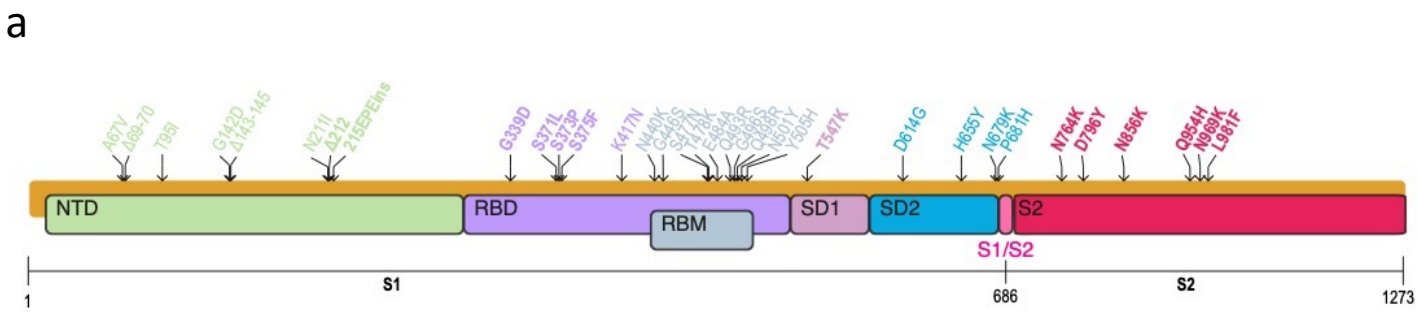

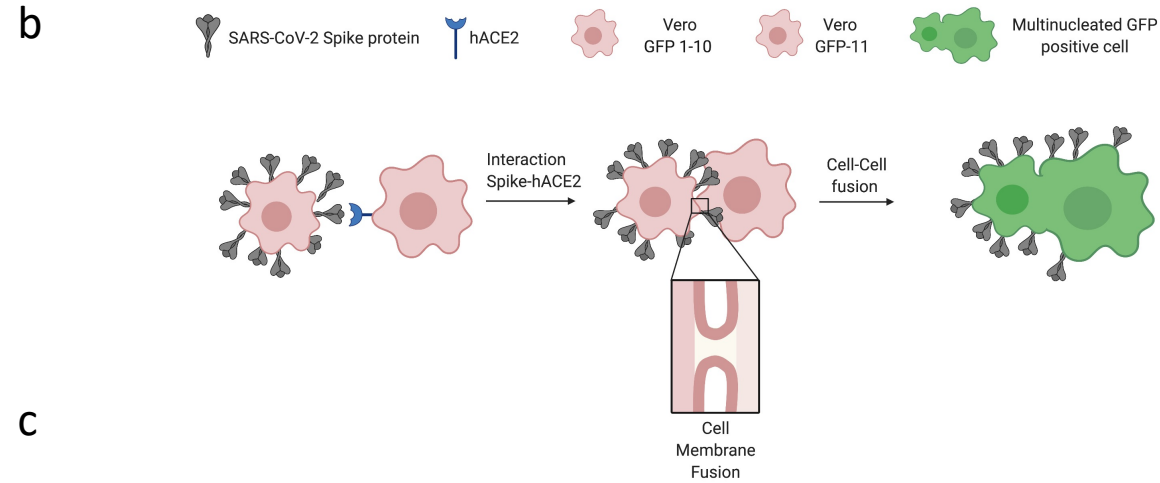

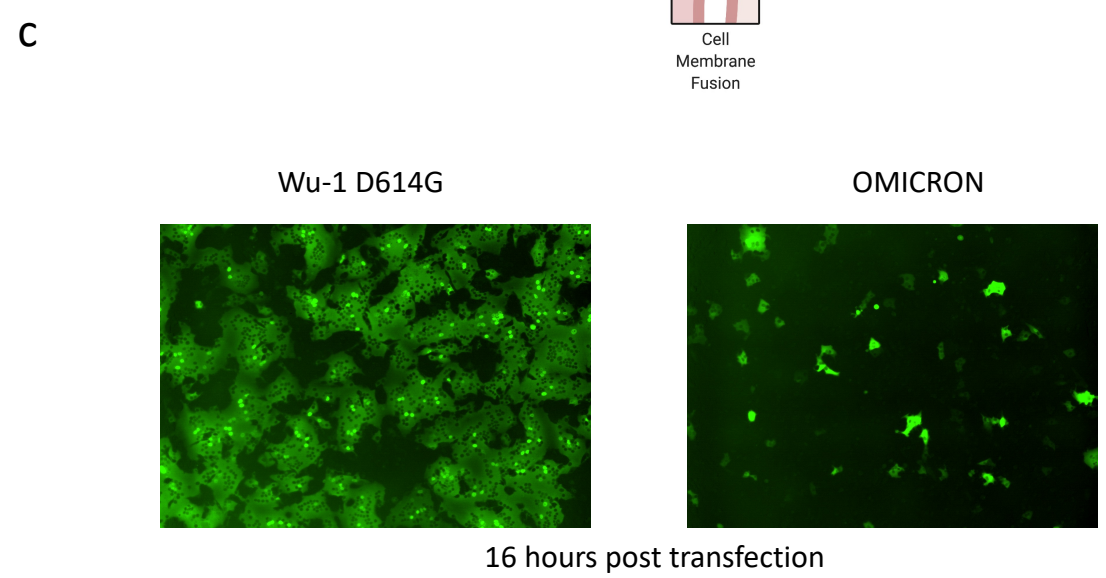

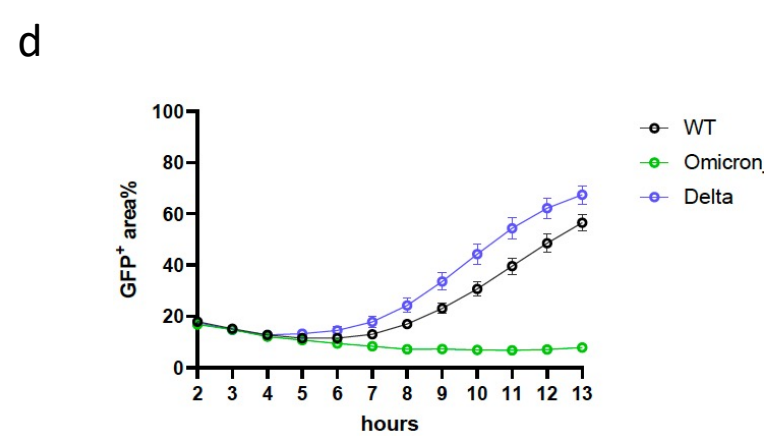

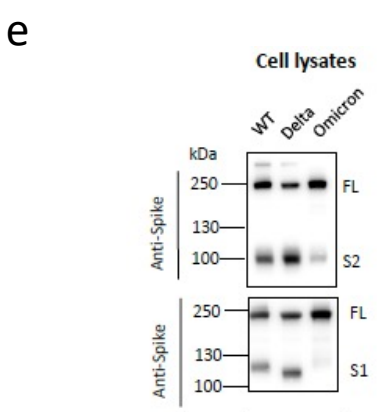

Figure 4: Omicron variant spike confers impaired cell-cell fusion activity. Graphical representation of Omicron B.A1 spike mutations present in expression plasmid used for fusion assay. Mutations coloured according to location in spike; bold mutations are novel to this lineage and have not been identified in previous variants of concern (VOCs). **b.** Schematic of cell-cell fusion assay. **c.** Reconstructed images at 16 hours of GFP+ syncytia. **d.** Quantification of cell-cell fusion kinetics showing percentage of green area to total cell area over time (WT is Wuhan-1 D614G). Mean is plotted with error bars representing SEM**. e.** western blot of cell lysates 48 hours after transfection of spike plasmids and lentiviral expression plasmids. Anti-S2 antibody. Data are representative of at least two independent experiments.

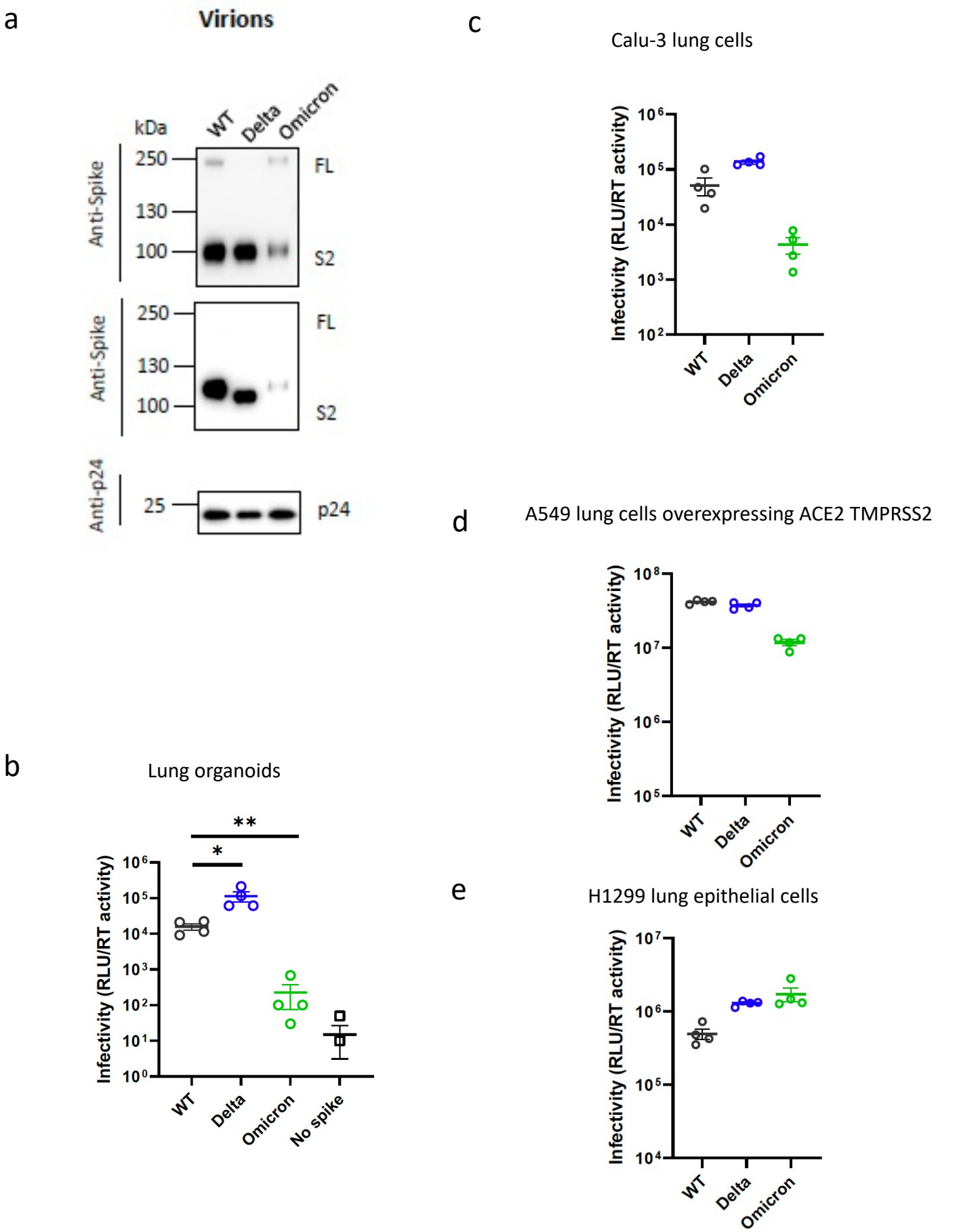

Figure 5: SARS-CoV-2 Omicron Variant spike mediated entry efficiency. a. western blots of pseudotyped virus (PV) virions from 293T producer cells following transfection with plasmids expressing lentiviral vectors and SARS-CoV-2 S plasmids. (WT- Wuhan-1 with D614G), probed with antibodies for HIV-1 p24 and SARS-Cov-2 S2 (top) and S1 (bottom). **b.** Single round infectivity on lung organoids using by spike plasmid pseudotyped virus (PV) produced in 293T cells **c, d,e.** Single round infectivity on Calu-3, A549 A2T2, and H1299 lung cells by spike plasmid PV produced in 293T cells. Data are representative of three independent experiments.